NASA SP-5957 (03)

TECHNOLOGY UTILIZATION

ANALYTICAL TECHNIQUES AND INSTRUMENTATION

A COMPILATION

NATIONAL AERONAUTICS AND SPACE ADMINISTRATION

Foreword

The National Aeronautics and Space Administration and the Atomic Energy Commission have established a Technology Utilization Program for the dissemination of information on technological developments which have potential utility outside the aerospace community. By encouraging multiple application of the results of its research and development, NASA and AEC earn for the public an increased return on the investment in aerospace research and development programs.

This document is intended to provide such technical information and is divided into three sections. The first section covers analytical instrumentation useful in the analysis of physical phenomena. Section Two is devoted to analytical techniques used to determine the performance of materials. The third section presents systems and component analyses for design and quality control.

Additional technical information on individual tools and techniques can be requested by circling the appropriate number on the Reader Service Card included in this Compilation.

The latest patent information available at the final preparation of this Compilation is presented on the page following the last article in the text. For those innovations on which NASA and AEC have decided not to apply for a patent, a Patent Statement is not included. Potential users of items described herein should consult the cognizant organization for updated patent information at that time.

We appreciate comment by readers and welcome hearing about the relevance and utility of the information in this Compilation.

Jeffrey T. Hamilton, *Director*
Technology Utilization Office
National Aeronautics and Space Administration

NOTICE • This document was prepared under the sponsorship of the National Aeronautics and Space Administration. Neither the United States Government nor any person acting on behalf of the United States Government assumes any liability resulting from the use of the information contained in this document, or warrants that such use will be free from privately owned rights.

For sale by the National Technical Information Service, Springfield, Virginia 22151. $1.00

For sale by the Superintendent of Documents, U.S. Government Printing Office, Washington, D.C. 20402

Contents

Section 1. Analytical Instrumentation

QUADRUPOLE ROD MOUNTING TECHNIQUE

A modified design provides greater sensitivity and structural stability in a quadrupole mass spectrometer used in analyzing the atmospheres of distant planets. This new technique reduces the stresses the vacuum and temperature of space impose on the spectrometer subcomponents.

The four hyperbolic rods that generate the quadrupole field are held together by straps in two ceramic ring-plates mounted on two flexure plates on either end of the rods. A dual-filament ion source is attached to one flexure plate. The source is aligned and the rods are maintained by the source nozzle and the ceramic plate. The electron multiplier is also mounted in a flexure-type mounting bracket, which effectively decouples the critical system components from the housing. This "floating" construction protects the spectrometer from vibration induced by external forces and keeps the internal components aligned.

The electron multiplier was redesigned to prevent neutral particles, passing through the quadrupole filter, from registering as a signal, thus decreasing background noise. This was accomplished by using the first dynode of the multiplier as an ion deflector to guide ions to the second dynode. Since the neutral ions are not deflected by electric fields, they continue on a straight line, impact the first dynode, and are eliminated. The field geometry between the first and second dynodes prevents any secondary electrons produced by the neutrals at the first dynode from entering into the second dynode area.

The quadrupole mass spectrometer developed in this program has outperformed any known device of similar size and design.

Source: The Perkin-Elmer Corp.
under contract to
Goddard Space Flight Center
(GSC-11407)

Circle 1 on Reader Service Card.

MASS-SPECTROMETER CALIBRATION FOR WATER ANALYSIS

A new stable water-calibration standard has been developed for mass spectrometers. For use in space flight, calibration standards must be stable and reproducible for up to one year, and they should require a minimum of space. Prior techniques required elaborate water-saturation cells with sophisticated ovens, flow paths, and equilibrators to insure that the water content of the calibration gas was known.

In this method, a reference standard is chosen to simulate water vapor in a mass spectrometer. It has the mass-to-charge ratio of singly ionized water vapor. This standard does not interfere with nitrogen, oxygen, or carbon dioxide analyses at their respective mass-to-charge ratios of 28, 32, and 44. The standard dideuteromethane (methand-D_2 or CH_2D_2) has been chosen, since it has a mass-to-charge ratio of 18 when singly ionized, and it is quite stable. The relative sensitivity of methane-D_2, when determined in the mass-spectrometer system in which the water calibration is required, amounts to 1.2 to 1 (methane-D_2 to water).

No maintenance of the system is necessary, since the gas composition forms a stable compound and can be mixed with dry nitrogen as a diluent gas. However, since methane-D_2 has chemical properties similar to normal methane, a mixture with oxygen or air may result in a flammable compound.

A related innovation is described in NASA Tech Brief B71-10466, "Metabolic Breath Analyzer".

Source: C. L. Perry
Marshall Space Flight Center
(MFS-22220)

Circle 2 on Reader Service Card.

OPERATION OF A NUDE QUADRUPOLE RESIDUAL GAS ANALYZER AT EXTENDED CABLE LENGTHS

Inside a vacuum chamber, the operation of nude quadrupole residual gas analyzer (RGA) beyond 1.3 meters (6 feet) from its externally mounted RF-dc generator is complicated by the fact that the RF oscillator circuits detune due to the coaxial cable reactance. This occurs because the quadrupole head acts as a capacitor in the RF-dc generator tank-circuit; any increase in cable length will detune the circuit, changing its frequency from resonance by changing its L-to-C ratio. The power required to operate the quadrupole RGA varies with the fifth power of the frequency and is directly proportional to the tank-circuit capacitance; the mass range varies inversely with the square of the frequency.

The operation of the nude quadrupole residual gas analyzer up to a distance of 61 meters (200 feet) from its RF-dc generator is made possible without altering the generator circuit by employing an RF link to drive the quadrupole rods. This RF-link technique adjusts the RF-dc generator independent of the cable length, because the lengths of the coupling coils at each end of the coaxial line are such that their reactance at the frequency used becomes equal to the characteristic impedance of the line.

The RF-dc generator supplies the proper voltage to the quadrupole rods. The dc-RF voltage ratio determines both the resolution and sensitivity of the quadrupole residual gas analyzer. As the dc and RF voltages are swept, ions pass through the quadrupole in order of increasing mass. The RF-dc generator is set by the manufacturer for the mass range of 5 to 250 atomic mass units at a frequency of 3.3 MHz.

The RF-dc generator can be modified by transferring the positive and negative dc voltage connections. (Figure 1, from points V and Y to points W and X, respectively.) These two voltages are then tapped from this new location and carried through the BNC connectors usually used for the RF voltages, where they are delivered to the quadrupole rods via the RF link. Since the length of the coaxial cable length going to the quadrupole head is not short compared to the wave length, it is necessary to treat the cable as a flat transmission line with inductive link coupling.

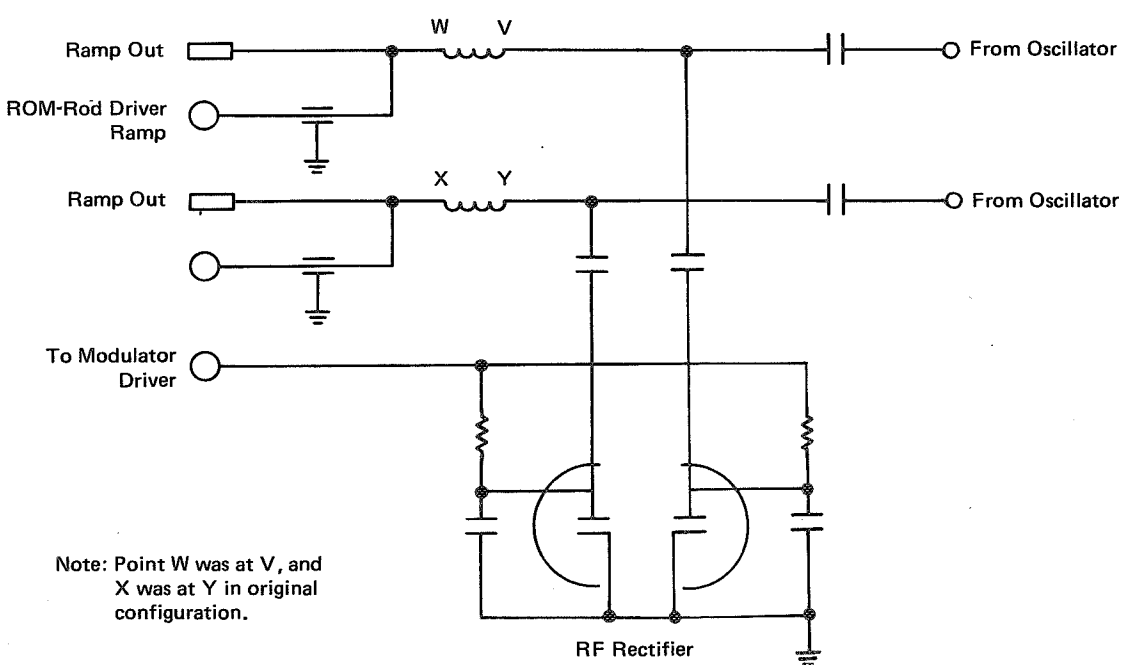

Figure 1. RF-dc Generator Modification

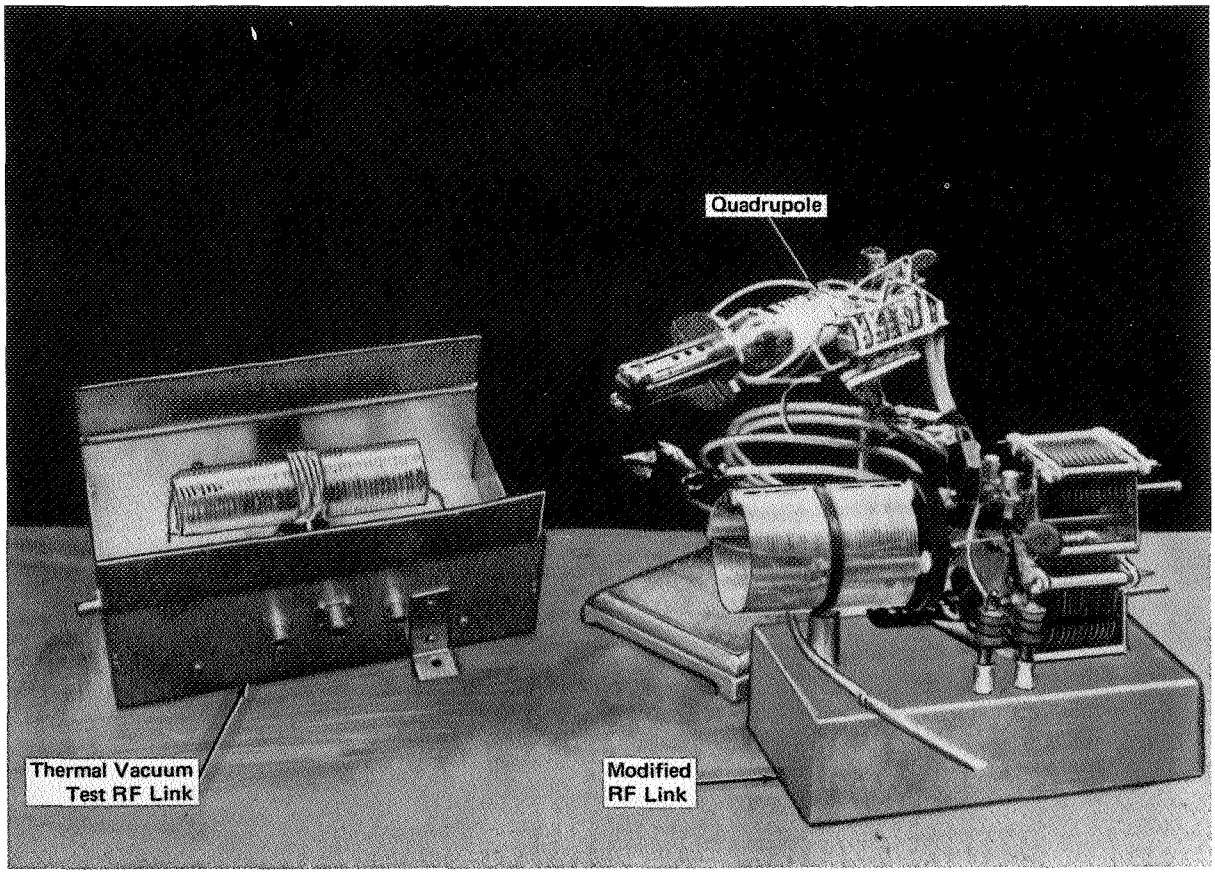

Figure 2. Quadrupole Analyzer

Figure 2 shows the hardware developed for the initial test and the modified RF link that enables the RGA to be employed at distances up to 61 meters from its RF-dc generator without modification to the generator circuitry.

This RF link technique should be of interest in the fields of mass spectroscopy, vacuum physics, nuclear reactors, thermal vacuum testing of space vehicles and atmospheric air pollution detection utilizing quadrupole residual gas analyzers.

Source: P. W. Tashbar and D. N. Nisen
Marshall Space Flight Center
(MFS-22147)

Circle 3 on Reader Service Card.

AUTOMATIC MICRODILUTION SYSTEM

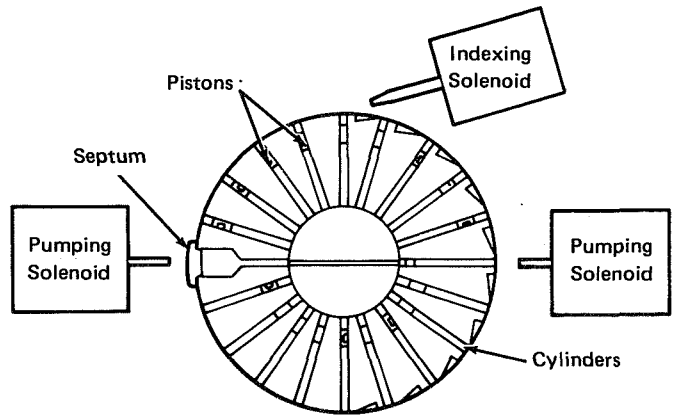

Figure 1. Automatic Dilution System

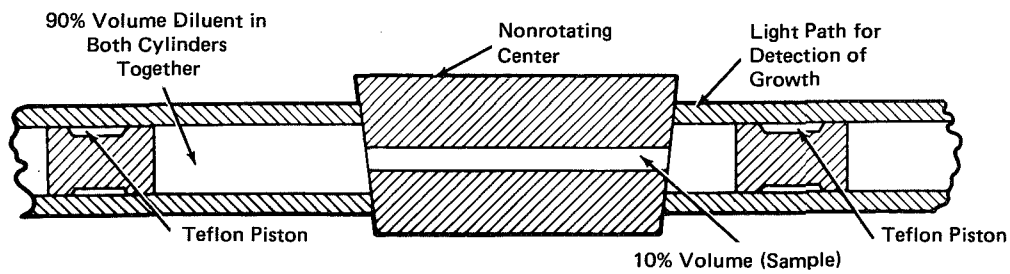

Figure 2. Cross-Section of Dilution System

There are several commercially available diluters in existence. Some use motor driven pistons or syringes and others use a calibrated capillary for the sample and a vial of diluent. In all these devices, the dilution must be accomplished in stages, and the diluted samples must be handled and transferred manually to detection chambers.

This diluting device operates on a stopcock principle. There are 10 pairs of cylinders in a rotating ring around a fixed center (see Figure 1). The center bore contains 10% of the sample volume, and 90%-diluent volume is stored in each pair of cylinders (Figure 2). The sample is injected through a septum into the center. The cylinder ring is then rotated to bring a pair of cylinders into line with the sample holder. The pistons are pushed back and forth by solenoid actuators on each side. The fluid motion, back and forth through the center, mixes the sample and diluent. After mixing, the cylinder ring is rotated to a new position for the next stage of dilution. When all nine stages of dilution are complete, the entire device can be placed into an appropriately designed spectrophotometer for sequential analysis of all dilutions.

The device is adaptable to either micro or macro quantities and may serve as part of an automated clinical chemical or microbiological analysis system.

The apparatus eliminates the problem of sterilization by being disposable. Handling is reduced to a minimum because the detection cells are built into the diluting device; decreasing the handling reduces the possibility of accidental leakage and exposure of personnel to pathogenic microorganisms. In addition, the device is relatively easy to manufacture.

Source: P. L. Nelson and
R. D. Howell of
McDonnell Douglas Corp.
under contract to
Johnson Space Center
(MSC-13412)

No further documentation is available.

GAS-CHROMATOGRAPHIC METHOD FOR ANALYSIS OF DISSOLVED OXYGEN

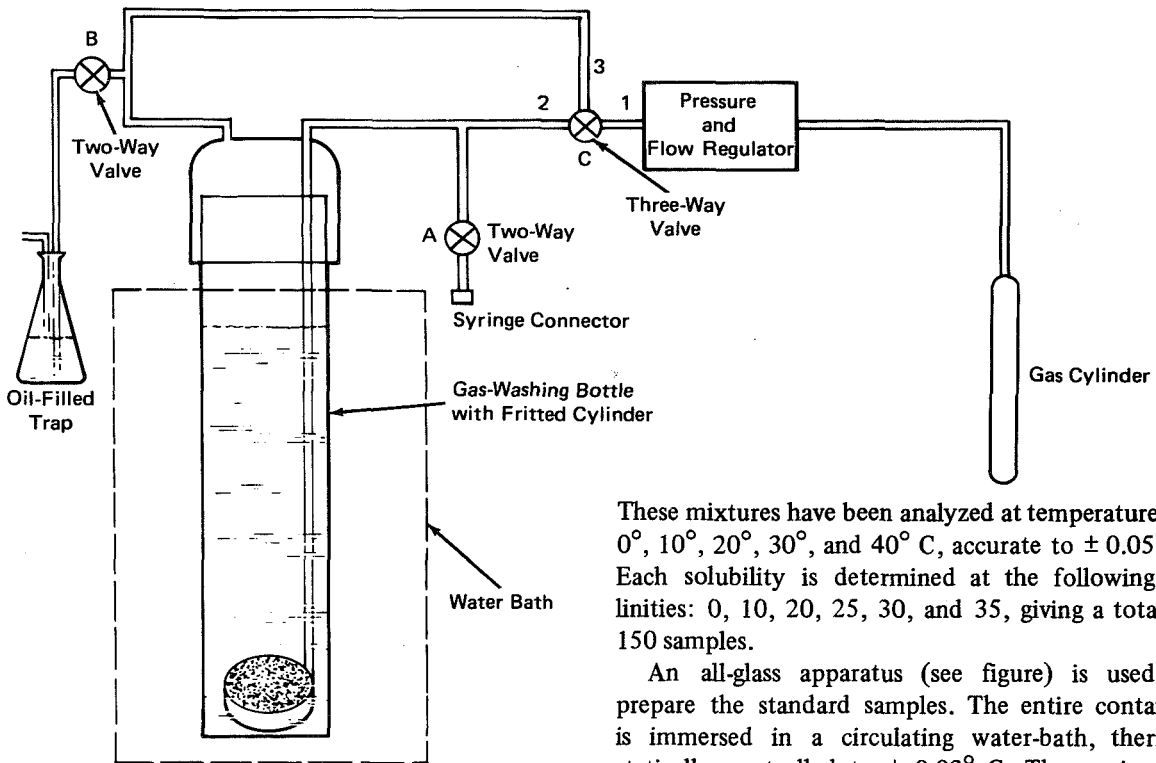

Apparatus for Saturating Water with Oxygen

Gas chromatography has long been used for the analysis of dissolved gases in water. However, a standard for the accurate calibration of dissolved oxygen measuring devices has been difficult to prepare. With the broad interest in water pollution, such a calibration standard should command wide attention among governmental and industrial organizations.

Because of the response characteristics of different measurement techniques, oxygen standards must span a range of salinities, temperatures, and concentrations of interest. A new standard oxygen solution for the calibration of dissolved oxygen measuring devices meets this requirement. Analyses of the following saturated solutions have shown the amount of dissolved oxygen present to be accurate to ± 0.05 ml-$O_2/_1$-N_2.

Gas Mixture	% Oxygen in Nitrogen
1	20.95
2	16.28
3	11.95
4	8.22
5	4.11

These mixtures have been analyzed at temperatures of 0°, 10°, 20°, 30°, and 40° C, accurate to ± 0.05° C. Each solubility is determined at the following salinities: 0, 10, 20, 25, 30, and 35, giving a total of 150 samples.

An all-glass apparatus (see figure) is used to prepare the standard samples. The entire container is immersed in a circulating water-bath, thermostatically controlled to ± 0.03° C. The equipment consists of two two-way valves, a three-way valve, a gas-washing bottle with a fritted cylinder, a syringe connector, and an oil-filled trap that prevents contamination from the atmosphere. Water of the desired salinity is placed in the gas-washing bottle, and the water bath is adjusted to the temperature of interest. The gas mixture is flowed through the system at 5 ml/min by adjusting valve C to flow in the direction of 1 to 2, with valve A closed and valve B open.

Under equilibrium conditions, a water sample may be taken for analysis. With valve B closed and valve A opened, valve C is turned to allow flow from 1 to 3. After all bubbles in the lines have been flushed out, a clean syringe may be connected to G and a sample taken.

Source: J. F. Whidby of
General Electric Co.
under contract to.
Marshall Space Flight Center
(MFS-22352)

Circle 4 on Reader Service Card.

TWO-STAGE GAS/PLASMA PROJECTILE ACCELERATOR

A new two-stage accelerator can propel projectiles (up to 1.6 mm in diameter) at velocities over 20 km/s. Because it can accelerate fairly sizeable projectiles at such high velocities, this system has been used to simulate meteoroids in the laboratory.

The projectile is accelerated in two stages: First, by a compressed lightweight gas such as hydrogen or helium, and then, by an expanding plasma. The accelerator is shown in Figure 1.

In the first stage (lightweight-gas accelerator), the projectile is placed at the end of a gas-filled pump tube. It is separated from the tube by a retaining diaphragm that holds the gas in the tube. At the beginning of the tube there is a deformable piston and a 30 caliber cartridge. When the cartridge is fired, the piston forces the gas up against the retaining diaphragm next to the projectile. As the gas is compressed, the pressure becomes so great that the diaphragm bursts, and the projectile is shot out of the barrel. The barrel of this first-stage accelerator also serves as part of the second stage: the plasma accelerator.

The plasma is generated (Figure 2) when a capacitor discharges a very high current through a thin aluminum foil between two electrodes (one is an annular electrode, the other, the barrel of the gas-stage accelerator, is a center electrode). Because the plasma consists of moving charged particles, it is acted on by the forces arising from the interaction of its current and the magnetic field of the center electrode. These forces push the plasma out of the generator and into the compressor coil.

As the plasma is forced into the conical compressor coil, it expands until it touches the coil. This establishes a current in the coil and creates a time-varying magnetic field along its axis. Since current is generated in the plasma, perpendicular to this magnetic field, there is a radially inward force on the plasma. As long as the discharge current from the capacitor is increasing, the plasma (which is increasing in quantity) is contained and compressed by the coil. When the capacitor current begins to decrease, the field in the coil decreases. This causes the current induced in the plasma to change direction, and the plasma is forced out of the coil.

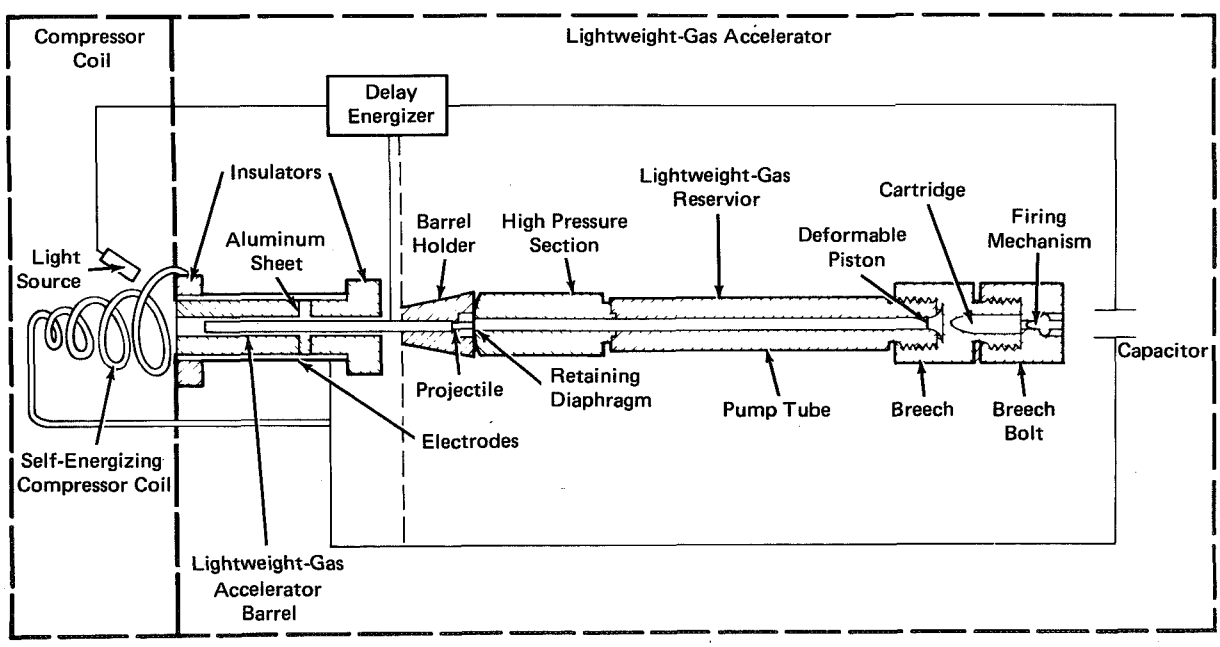

Figure 1. Lightweight-Gas Plasma Accelerator

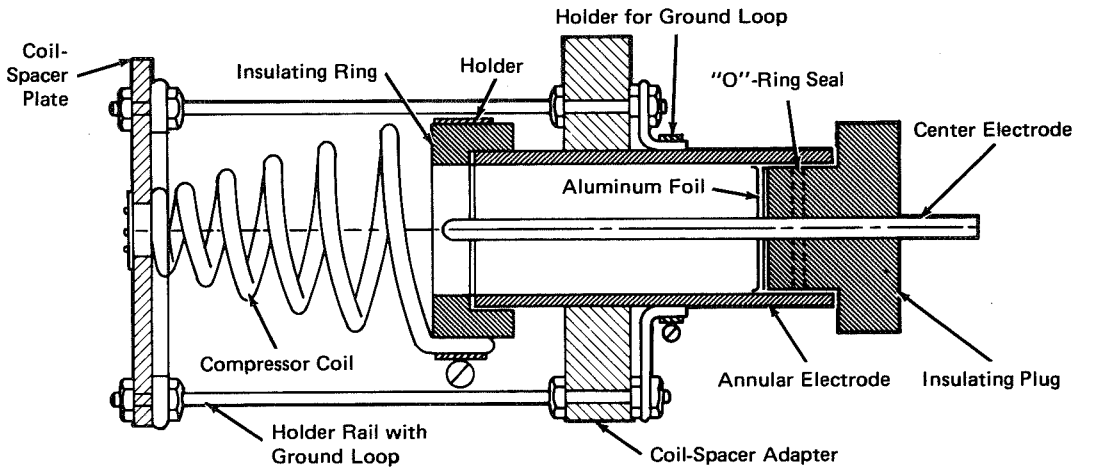

Figure 2. Plasma Compressor

To get the maximum accelerating force from the plasma accelerator, the projectile must be fired from the lightweight-gas accelerator to place it in the narrow end of the conical compressor coil at the time the plasma begins to expand. With the proper timing, velocities as high as those of the average meteoriod can be reached.

Source: E. L. Shriver, D. W. Jax and
D. W. Igenbergs
Marshall Space Flight Center
(MFS-22145, 22287)

Circle 5 on Reader Service Card.

DICHROMATIC ATTENUATION METHOD FOR DETERMINING BONE-MINERAL MASS *IN VIVO*

Bone-mineral mass has been estimated *in vivo* by the attenuation of X-rays from ^{125}I (photon energy of 128 KeV) in the limbs of astronauts before and after missions. The analysis of the data assumes that two types of tissue are present in the body: bone mineral and soft tissue. The attenuation of all soft tissues is assumed to be the same. In fact, however, soft tissues have many different attenuation characteristics. Adipose tissue, for instance, has a distinct attenuation coefficient. At 28 KeV it is about 80% of that of water. This causes as much as an 8% error in the estimate of bone-mineral mass of the radius.

A technique has been proposed to eliminate the error caused by adipose tissue present in the X-ray beam path. A second attenuation measurement is made at another photon energy. The modifications to the equipment are simple. A new source (^{153}Gd) with X-rays of two energies is substituted for ^{125}I, and two intensities are measured instead of one. This permits soft tissue to be distinguished from adipose tissue.

The feasibility of this technique has not been carefully evaluated because the intensity of the ^{153}Gd source is low, limiting the findings to statistical certainties of the measurement. But use of the dichromatic source, ^{153}Gd, for bone-mineral mass determination should eliminate bone-mineral mass-measurement errors caused by adipose tissue. Furthermore, this technique will permit the investigator to distinguish a change in adipose-tissue mass versus one in bone-mineral mass.

Source: J. R. Cameron and
P. F. Judy of
University of Wisconsin
under contract to
Johnson Space Center
(MSC-14276)

No further documentation is available.

Section 2. Analysis of Material Performance

INVESTIGATION TO IDENTIFY PAINT COATINGS RESISTIVE TO MICRO-ORGANISM GROWTH

An investigation was conducted to identify microbial-resistive paints or varnishes among the formulations used or evaluated for use as coatings on external surfaces of spacecraft. Spacecraft coatings are applied for various purposes, including passive thermal control, ionizing and optical radiation protection, radar reflectance, and protection of underlying metal surfaces from oxidation and corrosion. In addition to meeting such special property requirements, the coatings must have excellent adhesion, stability in the presence of thermal fluxes, and resistance to erosion from rain droplets and atmospheric particles.

Previously (NASA Tech Brief 69-10181), 166 coating formulations (most commonly, silicones and silicates) were identified and characterized with respect to their chemical and physical properties. Of the 166 formulations, 17 were subsequently selected as being representative of the coatings applied externally on spacecraft. The selected coatings were applied to carefully prepared aluminum alloy rods and evaluated in the laboratory to determine whether they were resistant to microbial attack and whether nutrients from the coatings were available for the growth of micro-organisms. It was found that all of the coatings contained nutrients that would support microbial growth or would allow survival of two or more species studied. Some of the coatings, e.g., fungicide-containing varnishes, a phenolic butyrate, and a polyimide, appeared to be somewhat resistant to microbial attack, while epoxy, acrylic, silicone, silicate, and polyurethane formulations, respectively, in decreasing order of resistance, appear to be more susceptible to attack.

The incorporation of suitable microbiocidal agents into selected coatings from the latter group is recommended for improved inhibition of micro-organism growth and for increased protection against deterioration of the coatings by micro-organisms. Research based on this recommendation could lead to the formulation of antimicrobial coatings for walls and equipment in hospitals and food processing plants, and the development of reusable, sterile polymer containers.

The following documentation may be obtained from:
National Technical Information Service
Springfield, Virginia 22151
Single document price $3.00
(or microfiche $1.45)
Reference: NASA-CR-111524 (N71-13017), Investigation of Spacecraft Materials that Support Micro-Organism Growth

Source: H. T. Kemp and C. W. Cooper of
Battelle Memorial Institute
under contract to
Marshall Space Flight Center
(MFS-20458)

FUSIBLE MATERIAL EVALUATION

A numerical analysis technique evaluates the performance of dual-fusion-point materials in heat transport systems. The energy storage characteristics are determined from the heats of fusion for the two phase changes, the phase-change temperatures, and the thermal capacitance. In an example, a heat sink used in a flowing-fluid thermal-control system is fabricated from a material with two phase-change points. The first phase change is from liquid-to-solid at 248 K (−14° F) with a heat of fusion (h_f) of 155 x 10^3 J/kg (66 BTU/lb). The heat sink contains 9.1 kg (20 lbs) of wax, requiring a total energy (E_p) to change phases at 248 K of: $h_f \cdot M = 155 \times 10^3$ J/kg · 9.1 kg = E_p = 1410 x 10^3 J (66 BTU/lb · 20 lb = E_p = 1320 BTU). The second phase change is a solid-to-solid change at 237 K (−34° F) with h_f = 42 x 10^3 J/kg and E_{pc} = 381 J (18 BTU/lb and E_{pc} = 360 BTU). Heat is transferred to the wax by convection and conduction. A typical energy temperature function E (T) is illustrated in the figure.

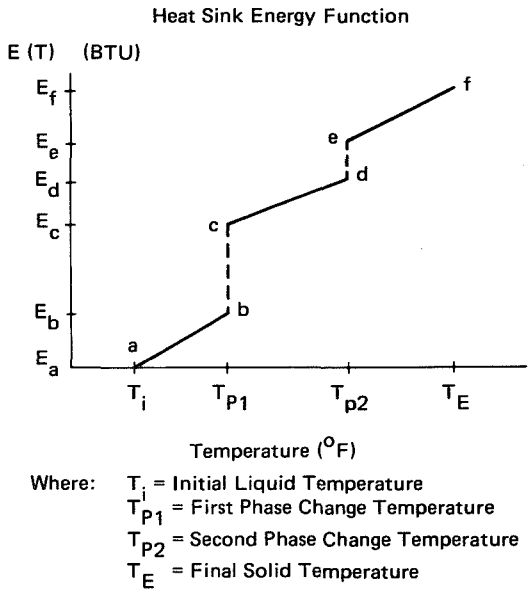

Source: C. E. Daniher, Jr., of
McDonnell Douglas Corp.
under contract to
Marshall Space Flight Center
(MFS-21810)

Circle 6 on Reader Service Card.

EXPLOSIVE/STAINLESS STEEL TUBE ANALYSIS

A mathematical model can be used to analyze the effects of explosive forces on confinement tubes. Model variables are: number and characteristics of the explosive strands, position of the strands within the confinement tube, size of the tube, and mechanical properties of the tube.

This technique has been used to evaluate explosive manifolds (tubes) on the Airlock Payload Shroud However, a similar approach with adequate adjustment for size, material, and explosive properties could be applied to other devices employing confined explosions. The analysis uses a combination of pressure-failure, constant-failure, and gas-expansion equations. It may be useful in designing confinement tubes for the containment of explosions in explosive activators, door releases, and emergency exits. The method provides an approximate solution that is more economical than existing multivariable computer programs.

Source: B. P. Kirk and E. C. Sulze of
McDonnell Douglas Corp.
under contract to
Marshall Space Flight Center
(MFS-21552)

Circle 7 on Reader Service Card.

EVALUATION AND OPTIMIZATION OF ADVANCED SIGNAL-COUNTING TECHNIQUES ON WELDMENTS

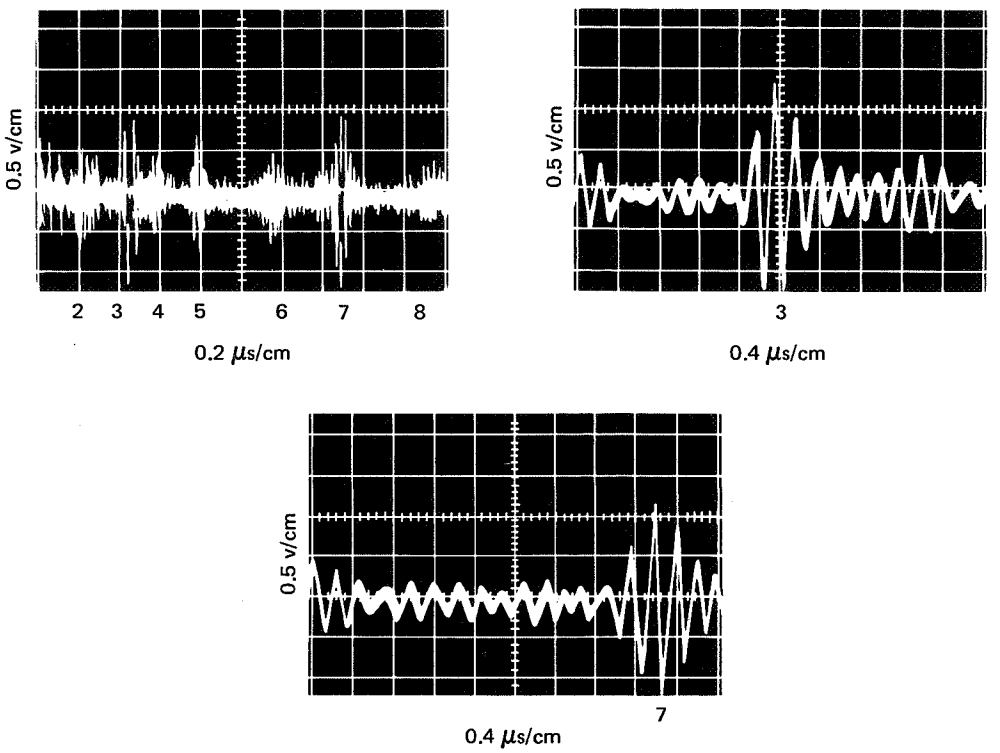

Raw Delta Scan Return from Fatigue Crack

This signal-counting technique augments the Delta method of ultrasonic test-signal processing in weldment-integrity analysis. Through exhaustive study, it has been found that for weldments of 1.27 cm (1/2 in.) or greater depth, this technique is superior to the conventional X-ray method.

At the present time, only the amplitude of a portion of the Delta scan signal is being used as a flaw indicator. In an attempt to utilize more of the information contained in the total signal an advanced signal-counting technique has been developed. It uses most of the received signal, requires uncomplicated and inexpensive electronic equipment, operates in parallel with the present amplitude-gate method, and has a digital output for direct insertion into a digital computer for further data processing.

The signal-counting technique operates by counting the number of oscillations in the received raw signal with excursions above and below a settable reference level, over a settable time span, or gating period. In practice, the reference level is set so that the background signal gives only one or two counts per gating period. The figure shows three raw Delta scan signals from a crack. The upper right and the lower traces show expanded (time) views of the signal at regions marked as 3 and 7. The signal at region 3 is the shear mode and at region 7 is the X mode. The upper left picture shows that there are at least 8 regions where the oscillations probably contribute to the total count.

Source: B. G. W. Yee, A. H. Gardner, L. Hillhouse, and D. R. Russell of General Dynamics under contract to Marshall Space Flight Center (MFS-22347

Circle 8 on Reader Service Card.

THERMAL CONDUCTIVITY AND ELECTRICAL RESISTIVITY OF POROUS MATERIALS

Thermal conductivity of porous material is an important property in determining the temperature distribution in a coolant and in the porous structure in transpiration cooling. Due to the irregularity of the microstructures, confident, theoretical calculation of thermal conductivity of porous materials is extremely difficult. Existing prediction methods are based on certain simplifications such as parallel cylinders, laminates in series, spheres dispersed in a conducting medium, etc. Even with a well-defined microstructure, the problem remains complex due to the existence of the interface resistance. Therefore, with the exception of parallel cylinders, a semi-empirical approach employing experimental data has been the only practical way of predicting the thermal conductivity of porous materials.

A study was conducted to provide experimental data of thermal conductivity and electrical resistivity of (1) woven and sintered mesh made from 304L stainless steel wire, (2) 304L stainless steel sintered spherical powder, and (3) OFHC (oxygen free high conductivity) copper sintered spherical powder. Three different porosities (0.093, 0.203, 0.385) of each material were tested from a temperature range of 100° C to 1000° C and the data tabulated in a series of tables and charts. The data were correlated into equations and compared with other published data and correlations.

It was found that the thermal conductivity, λ, and electrical resistivity, ρ, can be related to the solid material properties, λ_0 and ρ_0, and the porosity, ξ, of the porous matrix regardless of the matrix structure by the following correlation equations:

(1) For sintered powder and woven wire mesh, the dimensionless thermal conductivity can be represented by

$$\frac{\lambda}{\lambda_0} = \frac{1-\xi}{1+10\,\xi^2}$$

and the dimensionless electrical resistivity is given by

$$\frac{\rho_0}{\rho} = \frac{1-\xi}{1+11\,\xi^2}$$

(2) Within the temperature range where there is no magnetic transformation, the thermal conductivity of porous metals is related to the electrical resistivity and temperature, T, by the Wiedermann-Franz-Lorenz equation:

$$\lambda = \frac{LT}{\rho} + b$$

For a high conductivity material, the Lorenz constant, L, and the lattice component of conduction, b, are independent of porosity. For low conductivity materials, the lattice component depends on the porosity.

For low porosities, the calculated data compared well with published data and correlations. The departure of the high porosity data from existing correlations was cause for development of correlation equations applicable to the full span of porosities (0 to 100%). Utilizing only the experimental data of the above porous materials, full span correlations were developed. The published data of others covering the full span were then applied to the correlations in order to establish their validity throughout the span. The materials of others differed not only in matrix structure (e.g., foametal, feltmetal, and nonspherical sintered powders), but also in solid material properties. Such variances in material properties did not cause departures from the new correlations and proved the correlations applicable.

The following documentation may be obtained from:
National Technical Information Service
Springfield, Virginia 22151
Single document price $3.00
(or microfiche $1.45)

Reference: NASA CR-120854 (N72-19634), Thermal Conductivity and Electrical Resistivity of Porous Material

Source: J. C. Y. Koh of
The Boeing Company
under contract to
Lewis Research Center and
Anthony Fortini
Lewis Research Center
(LEW-11754)

ANALYSIS OF MICROSIZE PARTICULATES

Unique methods for analyzing individual particles ranging in size from 0.01 to 1000 micrometers have been developed for investigation of the nature of cosmic dust. The methods are also applicable to the particulate aerosols and contaminants characteristically encountered in studies of air pollution and in experiments with methods designed to abate pollution. Analysis of particulates is also of special interest in the forensic sciences.

The methods are nondestructive; as a result, single particles can be studied by a number of methods. For example, a particle as small as one micrometer may be mounted on a substrate or glass rod for X-ray analysis and then later remounted for another study. Analysis is routinely performed by combinations of transmission electron microscopy, scanning electron microscopy, electron-probe microanalysis, X-ray diffraction, optical minerology, and density measurement. Specimens larger than one micrometer are manipulated on a routine basis, and a computer program stores and retrieves data on all particles analyzed so that rapid analysis can be made for many parameters.

Considerable care must be exercised to ensure that samples are not contaminated by laboratory dust; all particle manipulation is performed in a clean room facility, meeting Federal Standard 209, Class 100 (fewer than 100 particles larger than 0.5 micrometer in every 0.028 m^3 [1 ft^3]). When particles are collected on the nitrocellulose film which usually overlays conventional electron microscope grids, laboratory contaminants are distinguished from collected specimens by a double-shadowing technique in which a thin metal film is deposited in a vacuum before and after particle collection; particles that were present before collection will have two shadows, but the collected particles will have only one.

Reference: M. B. Blanchard, N. H. Farlow, and G. V. Ferry: Methods of Analyzing Microsize Particulate Aerosols and Contaminants. Joint Conference on Sensing of Environmental Pollutants, Palo Alto, California, November 8-10, 1971, AIAA Paper No. 71-1104.

Source: M. B. Blanchard, N. H. Farlow, and G. V. Ferry
Ames Research Center
(ARC-10647)

FLAMMABILITY ANALYSIS OF NONMETALLIC MATERIALS IN AIR

This laboratory study was made to determine and compare the flammability characteristics of various nonmetallic materials of interest in the design of protective covers and fixtures for spacecraft interiors. A total of 33 materials were tested for the rate at which they self-extinguish while a gas flame is applied and after the flame is removed. (The burning rate in inches per minute, and those items that would not burn were noted.)

Two tests were used in the analyses: (1) American Society for Testing Materials (ASTM) D-568-1, "Flammability of Plastics 0.127 cm (0.050 in) and Under in Thickness" and (2) ASTM D-635-63, "Flammability of Rigid Plastics Over 0.127 cm (0.050 in) in Thickness." Nineteen items were analyzed by ASTM-D-568-1 and fourteen by ASTM-D-635-63. An average of 4.6 test specimens per item ignited.

Source: H. D. Peil of
Rockwell International Corp.
under contract to
Johnson Space Center
(MSC-17086)

Circle 9 on Reader Service Card.

MICROSAMPLE POUR-POINT DETERMINATION METHOD FOR FLUID LUBRICANTS

Fluid lubricants used in space or cryogenic applications must have very low pour points. A difficulty associated with the development of low-temperature lubricants is the lack of suitable definition of low-temperature flow characteristics. The long-established American Society for Testing Materials (ASTM) method D-97 "Cloud and Pour-Point Test" is somewhat inconvenient. Approximately 60 mil of product is required for the test, and in the case of experimental or developmental fluids, such volumes are frequently unavailable. In addition, the ASTM test has a repeatability of ± 5% and reproducibility between laboratories of ± 10%. At low temperatures (below 233 K), the accuracy is further reduced by difficulty in observing pouring tendencies through the rapidly icing pour-point jar wall.

This technique overcomes these problems. The analysis requires only 1 mil of sample. The sample is frozen to the side of a small test tube which is stoppered and tied vertically to a low-temperature thermometer. This assembly is immersed in a transparent-dewar cold bath and is brought to a temperature below the expected desolidification point. The cold bath is then warmed, and the temperature at which the sample moves a predetermined distance down the tube wall is taken as the pour-point. Because the tube and thermometer are immersed in a liquid bath, no visibility problem exists.

Source: M. N. Gardos of
Hughes Aircraft Co.
under contract to
Marshall Space Flight Center
(MFS-22413)

Circle 10 on Reader Service Card.

THERMAL PROPERTIES OF MATERIALS

This collection of thermal properties data concerns information on thermal properties of several materials related to the Space Shuttle Program. The materials are categorized as metallic, nonmetallic, insulators, and miscellaneous. Properties defined include density, thermal conductivity, specific heat, and emittance.

The metallic materials category consists of 2014-Tb and 2024-T4 aluminum, 6Al-4V titanium, Rene 41, L-605 and FS-85 columbium. Nonmetallic materials are polyurethane foam and fiberglass honeycomb, and the insulation materials category includes microquartz, dynaquartz, dynaflex, TG-15,000 and CS-1,000. Materials of the miscellaneous group are mullite HCF, zirconia HCF, carbon-carbon, foam ceramic, fluorinert, and R-512E coating for columbium.

This compilation of thermophysical properties of selected materials for spacecraft applications could be useful to commercial organizations involved in high-temperature design. Most of the data in the sections on nonmetallic materials, insulation, and miscellaneous materials are unique because the materials are either experimental or not generally available commercially.

Source: C. J. Goodbrake of
McDonnell Douglas Corp.
under contract to
Marshall Space Flight Center
(MFS-21899)

Circle 11 on Reader Service Card.

Section 3. Systems and Component Analysis

MAINTAINABILITY ANALYSIS PROCEDURES

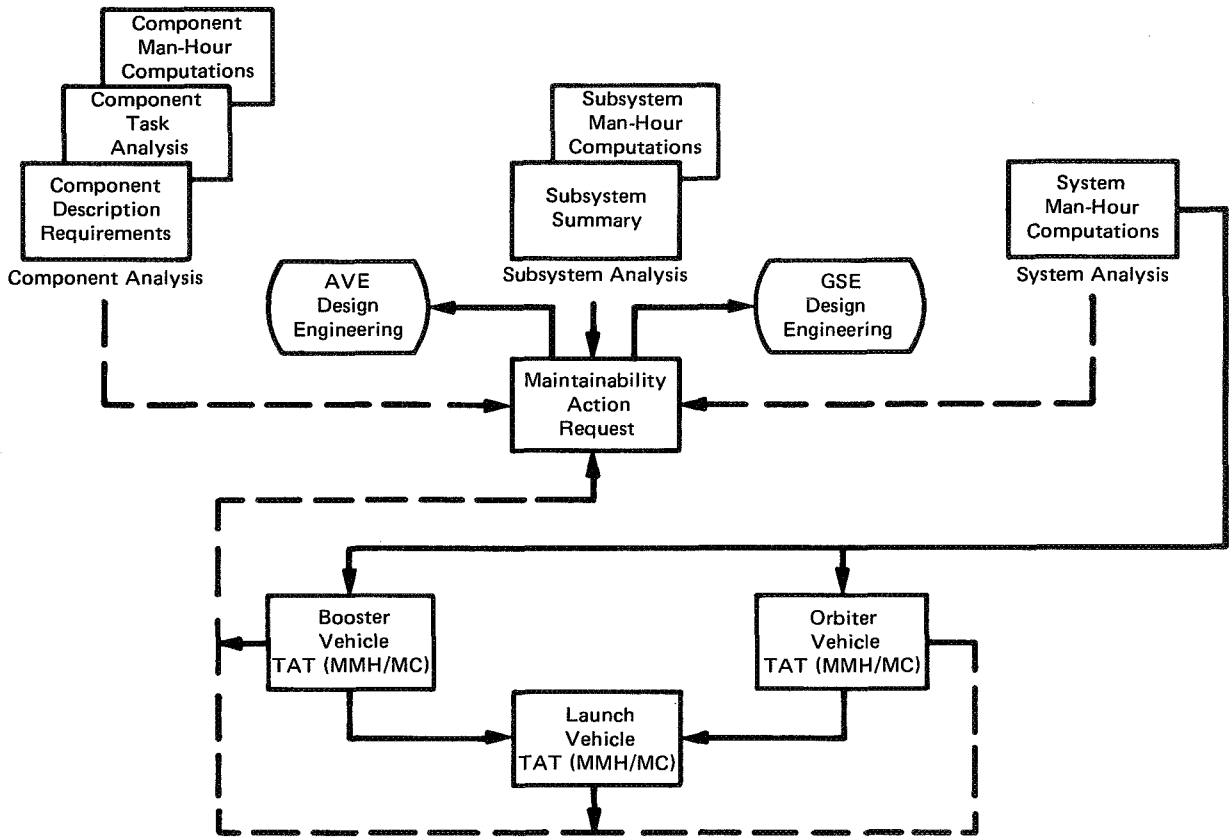

Flow Chart for Maintainability Analysis Procedures

This maintainability analysis establishes a standard for recording the results of the maintainability (M) analysis of the complex problems of a major space program. The procedures are clearly defined, presented in an orderly sequence, and provide the analyst with a step-by-step approach in the performance of an M analysis (see figure). Well planned individual control forms are used to record all of the analytical processes (see figure) used to arrive at the maintenance man-hour per flight hour (MMH/FH), maintenance man-hour per maintenance cycle (MMH/MC) related to turnaround time (TAT), personnel and skills required, etc. All these factors are fed into the aerospace vehicle equipment (AVE) and the ground support equipment (GSE) design engineering areas.

Various commercial, military, and aerospace approaches to M analysis for the different phases of a program are studied. Procedures are formulated to compile a compact data base with maximum output capabilities. With this combination, these procedures should satisfy the M analysis requirements of any agency to cover any program phase.

Source: R. E. Moon of
McDonnell Douglas Corp.
under contract to
Marshall Space Flight Center
(MFS-21865)

Circle 12 on Reader Service Card.

PRODUCIBILITY CONSIDERATIONS IN DESIGN

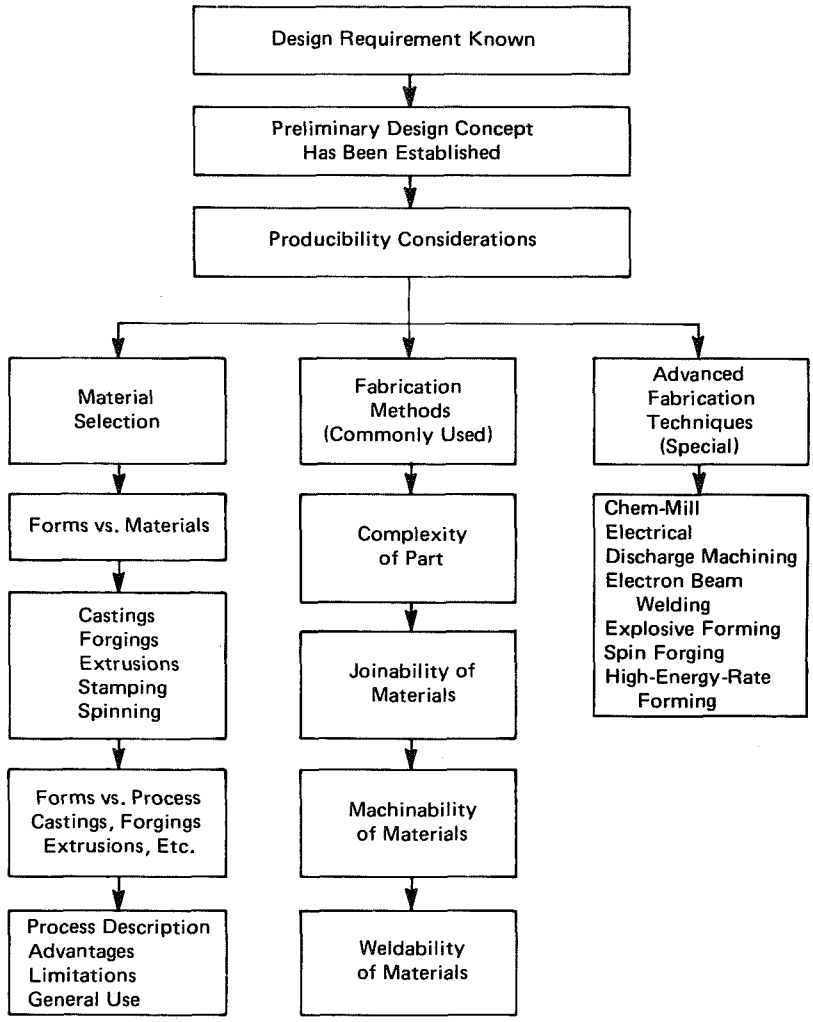

Producibility Considerations in Design

A single-source technical document is a useful reference for design engineers. This reference was prepared for aerospace design and manufacturing, but should be applicable to other industries as well. It contains guides for selecting the type of material, process, and fabrication method that will result in the optimal quality and cost effectiveness. The flow chart shows the general approach set forth in the document.

Source: M. L. Marke and E. V. Gillaspy of
Rockwell International Corp.
under contract to
Johnson Space Center
(MSC-17837)

Circle 13 on Reader Service Card.

EFFECT OF SIZE ON CRACKING OF MATERIALS

A new theory explains the effect of physical size of a specimen on crack propagation in any material. The brittle behavior of large mild-steel elements, the plasticity recently shown to exist in glass, and the marked size sensitivity of fatigue specimens are presently little understood phenomena. These and other unexplained observations are actually manifestations of a single law, termed the Strain-Energy Size Effect.

The effect of a specimen's physical size on the initiation of cracking in any material occurs in accordance with the statistics of flaw distribution. However, the effect of size on complete fracture is also dependent on the stability or instability of crack propagation.

Cracks can stabilize because of energy dissipation, load relaxation, or crack orientation; the former results from the physical properties of the material. The energy dissipation stability is affected by the strain-energy content (and therefore by the size) such that the higher the energy, the earlier this stability transforms into instability. Consequently, the larger the specimen, the lower the breaking stress and ductility that accompany cracking. A possible explanation is presented in terms of dynamic effects caused by an excess in the energy released over the energy absorbed. These dynamic effects influence the stability of the propagating crack such that the size of the specimen plays a dominant part.

The conditions favoring instability are: (1) small capacity for dissipating potential energy; (2) inclusions and voids at all levels of aggregation and coarseness of grain; (3) extremely thin and short existing cracks; (4) small capacity for damping vibrations; and (5) large size relative to other conditions.

From the viewpoint of cracking behavior, materials can be classified into three broad groups: ductile (mainly soft metals), semiductile (materials such as concrete and gypsum), and brittle (glass and similar materials). The two material constants required for the complete description of the material's resistance to fracture are: (1) the surface tension, γ; and (2) a higher constant, which represents the ultimate resistance to fracture and is usually denoted as G_c for the less brittle materials.

In cracking, a material goes through two critical phases. The initiation of the first crack is governed by a constant whose dimensions are equal to, but whose value is much less than G_c. In glass, this initiation constant is γ. In metals, no experimental evidence exists to indicate what value this constant has in relation to γ. Therefore, a new value γ' is defined as the limiting value that (1/2) G_c will approach as the specimen size increases to infinity (under these conditions $G = 2\gamma$). For glass, $\gamma = \gamma'$. Similarly, the upper constant G_i is defined as the limiting value that G_c will approach as the specimen size decreases to zero.

Thus, γ' should be the true design criterion for very large scale members. For ordinary sized members, it is important because it determines the event of crack initiation. Similarly, G_i should be the true design criterion for small elements of glasslike materials.

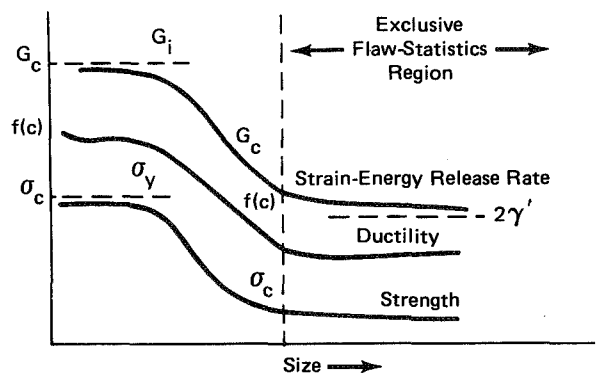

Figure 1. Size Dependence of Strength, Ductility, and Strain-Energy Release Rate of a Material

All curves representing the size dependence of strength and semiductility (i.e., the ductility accompanying cracking) have the characteristic shape of a reversed sigmoid (see Figure 1). This figure also shows the effect of size on G_c, as well as the limiting values of G_i and γ'. The difference between the two plateaus in each of the three curves is equal to the strength, the ductility, and the G_c value that would be gained during the stable propagation of a crack in an extremely small specimen of the material.

In principle, all materials exhibit the behavior described. They vary, however, in both the magnitude of the transition and its position. Figure 2 illustrates this difference in approximate terms.

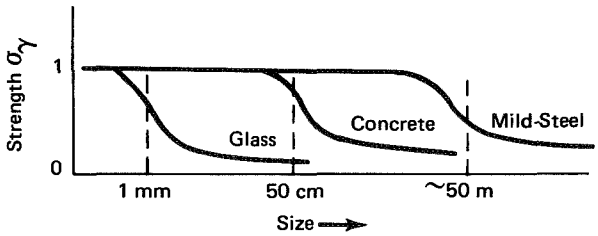

Figure 2. Transition Size for Some Typical Materials

Reference: JPL Technical Report 32-1438, Strain-Energy Size Effect

Source: J. Glucklick of
Technion-Israel Institute of Technology at
Caltech/JPL
under contract to
.NASA Pasadena Office
(NPO-11602)

Circle 14 on Reader Service Card.

MATHEMATICAL TECHNIQUES FOR ESTIMATING OPERATIONAL READINESS OF COMPLEX SYSTEMS

A report entitled "Mathematical Considerations of Operational Readiness" has been prepared as a guide for systems analysts. The report uses concepts from probability theory to develop methods of predicting operational readiness for a complex system. Use of the presented methods will aid engineers in the design of systems that offer an improved chance of mission accomplishment.

Operational readiness in this context is defined as the probability that a system can meet an operational objective during a prescribed interval of time, provided that some minimal maintenance can be carried out. The report introduces a well-known concept of the mean-time-between-failures or MTBF and presents an evaluation of its lower limit. Based on this lower limit which is estimated from the Chi-Square distribution, the designer can introduce an adequate number of spares to the system to improve its probability of operational success. The number of spares required is computed from the Poisson distribution.

The report includes a Poisson formulation for a parallel spare arrangement and expands to a more complex series-parallel configuration. The latter involves a system of linear, simultaneous, differential equations which are solved by the use of a Markov reliability matrix and Laplace transforms. Based on these operations, total system reliability is estimated. Maintenance probability, using the mean-time-to-repair (MTTR) concepts, and exponential distributions are also included in this report in addition to the expected number of failures in a given mission time.

In concluding the report, a hypothetical ground support equipment (GSE) subsystem is taken through the countdown sequences. The data used have been taken from actual GSE equipment, and the countdown time is given as 97 hours.

The report presents all the pertinent data for evaluation and shows the results of readiness probability computed by the above methods. All computations are performed by use of lower limits of MTBF's and upper limits of MTTR's.

Source: Ives D. Jacquier and Paul A. Miltz of
Rockwell International Corp.
under contract to
Johnson Space Center
(MSC-17694)

Circle 15 on Reader Service Card.

CAVITATION DATA FOR HYDRAULIC EQUIPMENT

Calculations and tabulated data of cavitation B-factors have been developed for helium, parahydrogen, nitrogen, fluorine, oxygen, refrigerant 114, and water. The B-factor is the ratio of the vapor volume to liquid volume that would exist if a given mass of fluid, which was initially all liquid, were expanded to a larger volume without heat addition. It can be interpreted as an indicator of the extent of "vapor lock" that can occur in a liquid pump or system. In pumps (and other flowing systems), there is an upper limit to the ratio beyond which the performance of the pump (or system) is impaired because of excessive cavitation. Once the relationship between performance and B-factor has been established for a particular pump (or system) for one fluid, its behavior for another fluid is also known. Most fluids, even complex fluids like freon, behave in a similar manner from the cavitation or boiling considerations.

A brief history is given on the development of the B-factor concept and its application to the design of liquid pumps. Previous methods of computing B-factor were reviewed and a simplified, more precise computation method was established.

The basic equation to determine the B-factor is:

$$B = \left(\frac{\rho_{f2}}{\rho_{v2}}\right)\left(\frac{m_{v2}}{m_{f2}}\right) = \left(\frac{\rho_{f2}}{\rho_{v2}}\right)\frac{s_{f1} - s_{f2}}{s_{v2} - s_{f1}}$$

where:

B = vapor to liquid volume ratio
m = mass
s = specific entropy
ρ = density
f1 = saturated liquid conditions at initial pressure
f2 = saturated liquid conditions at final pressure
v2 = saturated vapor conditions at final pressure.

This expression does not rely upon summation of incremental steps to account for changing fluid properties, vaporization of liquid, or recondensation of vapor. The B-factor resulting from any finite pressure (or corresponding temperature) depression may be calculated in one simple step. The accuracy of the results is limited only by the accuracy of the liquid pressure-volume-temperature (P-V-T) data, and charts, tables, etc., may easily be developed from appropriate equations of state or tabulated thermodynamic properties.

Almost the entire saturated liquid temperature range was covered for each fluid, i.e., from temperatures just above the triple-point to temperatures just below the critical point. Under normal circumstances, the value of B-factor does not exceed a value of 5.0 without incurring excessive cavitation. However, in order to insure complete coverage of the range that might be encountered, even under unusual circumstances, the computations for each fluid were made to B-factors of at least 10.1. These computations were made at intervals of bulk fluid saturation temperature which are sufficiently small to permit interpolation to intermediate temperatures. The tabular data presentation was chosen because it provides in the most concise form the maximum temperature range, B-factor range, and precision at close initial-temperature intervals. Graphs of the desired range and precision may quickly and easily be constructed from the tabulated data.

Graphs may be constructed from the tables to determine the intermediate B-factor functions, or interpolations may be made directly from the tables. An example problem is given, demonstrating the use of the tabulated data.

The following documentation may be obtained from:

Superintendent of Documents
U.S. Government Printing Office
Washington, D. C. 20402
Price $1.00

Reference: NBS Technical Note 397 (SD Catalog No. C13.46:397), Tabulated Values of Cavitation B-Factor for Helium, H_2, N_2, F_2, O_2, Refrigerant 114, and H_2O

Source: J. Hord and R. O. Voth of
National Bureau of Standards
under contract to
Lewis Research Center
(LEW-11642)

A METHOD FOR CALCULATING THE EFFECTS OF DESIGN ERRORS AND MEASUREMENT ERRORS ON PUMP PERFORMANCE

A method has been developed for calculating the effects of design errors and measurement errors on pump performance. Error equations and charts are utilized to relate the amount of error in a given performance parameter to the amount of error in a given design or measured variable.

Calculation of the effect of design errors is useful in pump design. It can show the sensitivity of a given design to design errors and manufacturing tolerances. It can be used to estimate the precision of a design, i.e., the limits around the design point within which the pump performance may be expected to lie with reasonable certainty. An analysis of the effect of errors can also show which step in a design procedure is the most critical source of error.

Calculation of measurement errors is important in evaluating pump test data. Mathematical techniques can be applied to analyze the effects of measurement errors on pump performance parameters. Using these techniques the amount of error to be expected in performance parameters can be calculated from estimates of the errors introduced by different measurements. An error analysis can also be used in planning instrumentation by showing which measurement is likely to introduce the largest errors.

In comparing design performance with measured performance, both design errors and measurement errors must be considered.

The error equations were derived primarily for axial flow pumps, but are not limited to axial flow. All of the design error equations and measurement error equations are correct for mixed-flow impellers and centrifugal pumps if the meridional velocity is substituted for axial velocity. However, the error equations apply to a design system and test procedures which are standard for axial flow pumps, but are not always used for mixed-flow impellers. The equations, as written, apply to rotors but can be modified for application also to stators.

The following documentation may be obtained from:

National Technical Information Service
Springfield, Virginia 22151
Single document price $3.00
(or microfiche $1.45)

Reference: NASA TN-D-5919 (N70-33164), An Analysis of the Effect of Design and Measurement Errors on Pump Performance Parameters

Source: D. A. Anderson
Lewis Research Center
(LEW-11503)

INVESTIGATIONS OF A TURBULENT JET IN A CROSSFLOW

Several aspects of the flow field downstream of a jet directed at right angles into a crossflow were studied experimentally. Single jets, both heated and unheated, were injected into a uniform, ambient temperature crossflow. Ratios of jet momentum to crossflow momentum ranged from 16 to 64. Longitudinal and transverse distributions of velocity, temperature, and turbulence intensity were measured at distances up to 70 nozzle diameters downstream from the injection plane.

In recent years, considerable attention has been given to the various aspects of jets issuing into a subsonic crossflow since this is the basic configuration in numerous situations of significant concern, such as:

1. Cooling of hot gas streams by the injection of jets of cool gas, e.g., cooling gas turbine combustor exit gases by injecting cooler air through holes in the liner wall;
2. The aerodynamic effects of propulsion system jet flows on the performance of STOL and VTOL aircraft;
3. The distribution of contaminants discharged from a chimney into the wind; and
4. The distribution of contaminants discharged into flowing water.

This investigation was motivated by the gas turbine combustor gas cooling problem. Although multiple jets are used in actual applications, the injection of a single jet into a semi-infinite crossflow is a basic component of the system. The results obtained from this study provide basic information not only for the combustor cooling problem, but also for many other applications.

Detailed aspects of a jet injected into a crossflow of the same temperature were investigated first to better understand the mixing process. Distribution of velocity, pressure, and turbulence intensity were measured at several sections in the jet. The data revealed a complex structure of the jet, strongly influenced by a pair of counter-rotating eddies which are formed behind the jet. Therefore, the rotational velocity field was also investigated in detail.

The mixing of the two flows at different temperatures was investigated by heating the jet above the temperature of the crossflow. Although the buoyancy force acts in opposite directions in heated and cooled jets, this effect does not significantly alter the general flow characteristics. Lateral distribution of temperature at several sections of the jet and longitudinal distribution of temperature along the centerline of the jet were measured in detail to study the mixing of the two flows.

These experiments showed that for both heated and unheated jets, velocity trajectory depends solely on the ratio of jet momentum to crossflow momentum. Jet temperature trajectory, defined by the locus of the maximum temperature difference in the plane of symmetry, was found to be mainly dependent on the momentum ratio, with a weak dependence on density ratio indicated. The twin vortex motion was found to grow stronger with increasing momentum ratio; in heated jets the vortex motion is also influenced by the density ratio. The vortex activity attains its peak in the region where the jet centerline has large curvature and decays rather slowly thereafter. The higher entrainment rate of a jet in a crossflow as compared to a free jet is largely due to the normal component of crossflow velocity.

The following documentation may be obtained from:
National Technical Information Service
Springfield, Virginia 22151
Single document price $3.00
(or microfiche $1.45)
Reference: NASA CR-72893 (N71-29896), Experiments on a Turbulent Jet in a Cross Flow

Source: Y. Kamotani and I. Greber of
Case Western Reserve University
under contract to
Lewis Research Center
(LEW-11680)

ANALYTICAL METHODS FOR BACTERIAL KINETICS STUDIES

Analytical methods for studying the kinetics of bacterial growth and metabolism, utilizing mathematical equations and models and specialized computer techniques, have been reported. This study of bacterial kinetic activity is applicable to fields as far ranging as food production, complex chemicals production, and polluted water purification. Through the methods developed, a better understanding of such activity can be achieved, greater control over the processes involved can be made possible, and optimal process conditions over a broad range of variables can be predicted.

The computer technique described is applicable to the analysis of batch-culture kinetic data and is used for fitting equations to the data. The equations can then be used for data interpolation, extrapolation, integration, differentiation, and other manipulations.

The data in the report were obtained with a salt-tolerant strain of sulfate-reducing bacteria grown in both batch and continuous cultures. The results of the computer analysis of this data are discussed in relation to some of the proposed mathematical models. The report also includes a description of a novel continuous-culture apparatus used in these experiments.

The apparatus used for measuring bacterial cell size-concentration distributions employs a measurement technique which differentiates between normal cells and heat-killed cells: A result that should be of considerable value in the study of bacterial sterilization kinetics. The apparatus was calibrated and used in obtaining information on the cell size under a variety of experimental conditions. A computer program was used to analyze the computer-coupled output.

The following documentation is available from:

Technical Information Division
Lawrence Radiation Laboratory
University of California
Berkeley, California 94720

Reference: UCRL-16398, Analytical Methods in Bacterial Kinetics

Source: V. E. Edwards and C. R. Wilke of
Lawrence Berkeley Laboratory
(LRL-10011)

Circle 16 on Reader Service Card.

EXPERIMENTAL ANALYSIS OF LOW-PROFILE FLANGE CONNECTIONS

A comprehensive experimental investigation of low-profile bolted flange connections includes a qualitative examination of surface stresses by means of brittle lacquer and photoreflective techniques. In addition, a three-dimensional photoelastic analysis of an epoxy model is described using the stress-freezing method. A strain gauge analysis at selected points on the model is also presented.

Based on the results of the investigation, it is concluded that the low-profile flange is a basically sound design. It has only low levels of stress concentration except in the area immediately beneath the flange bolt heads. Flange depth and bolt spacing provide an even distribution of stress as the flange-to-gasket interface. The geometric design and the flexibility of the gasket have a significant effect on the stress distribution in both the flange and adjacent pipe section. Furthermore, stress concentrations under the flange-connection bolt heads could be reduced by shaped washers or by separate bolting rings.

Source: W. K. Kabitza and
G. L. Hearne of
University of Alabama
under contract to
Marshall Space Flight Center
(MFS-22109)

Circle 17 on Reader Service Card.

THE DESIGN OF AN AUTOMATED VERIFICATION OF REDUNDANT SYSTEMS

A handbook, entitled "Design of Automated Redundancy Verification," has been published as a guide to designers who work with redundant systems. The handbook presents a general systems approach to this topic in which it discusses design methods for automated redundancy verification systems.

The design approaches described depend on the characteristics of the "item being verified" (IBV), which is any system requiring automated redundancy verification. In general, there are three approaches to indicate the status of IBV, i.e.: whether the redundancy is present or not, whether the item is working or not, or whether the redundancy complement has degraded from, for example, three to two. In all cases, verification is in a discrete form. The verification in the first case requires a form of "present" or "not present." In the latter two, the verification takes forms of "go" or "no go" or the green, amber, and red.

The handbook provides the following:

1. It describes the design processes.
2. It presents step-by-step design considerations with appropriate design techniques.
3. It gives a sufficient amount of tutorial material on implementation and methodology.
4. It shows design aids in the form of charts and graphs for ready reference.
5. It illustrates the use of each design aid in addition to application examples of the overall process.
6. Finally, it discusses design guidelines and identifies general practices to be adhered to or avoided.

The following documentation may be obtained from:
National Technical Information Service
Springfield, Virginia 22151
Single document price $3.00
(or microfiche $1.45)
Reference: NASA-CR-125311 (N72-15228) Handbook-Design of Automated Redundancy Verification

Source: F. A. Ford, T. W. Hasslinger, and F. J. Moreno of Systems Division of Radiation, Inc. under contract to Kennedy Space Center (KSC-10702)

LOUDNESS (ANNOYANCE) PREDICTION PROCEDURE FOR STEADY SOUNDS

A method has been devised to predict the loudness level of any steady sound solely from its measured power-spectrum level. For many applications, hand calculations are adequate; however, for applications involving considerable data, a computer program has been written to perform the loudness-level computation when the data consist of a 1/3-octave, power-spectrum-level analysis of the noise (see Note). The method is based on the assumption that, with respect to the loudness sensation, the human auditory system acts as an open loop transmission system with a transmittance function determined from well-known, input-dependent, equal-loudness curves which are obtained by exposure of listeners to pure tones. (This differs from present methods wherein the transmittance function is often assumed to be independent of the stimulus intensity and is based on equal-loudness curves obtained by exposure to imprecisely specified bands of noise.) The transmitted power-spectral density is summed over all frequencies to obtain the overall loudness (annoyance) level. (This differs from most methods wherein loudness, rather than power of frequency bands, is summed over all bands to obtain the overall loudness.)

Because the sensations produced by sound stimuli in human beings are important to human existence and the development of human intellect, it is imperative in many endeavors ranging from sound reproduction (e.g., broadcasting) to transportation (e.g., pollution by noise) that the magnitudes of the sensations be quantified.

Any word which a listener might use to describe the subjective sensation produced by a sound constitutes a description of a psychological sensation which might be quantifiable. Possibly the most widely recognized auditory sensation is "loudness." Loudness is defined as the magnitude of the auditory sensation produced by a sound stimulus. For annoying sounds, loudness is often a good measure of annoyance as well.

The loudness of all sounds is specified relative to that of a 1-kiloHertz tone imposed on a listener from the front, as plane waves at a sound-pressure level of 40 decibels. This reference sound and any other equally loud sound is said to have a loudness of 1 "sone." Like sound pressure, loudness is often expressed in logarithmic form and called loudness "level." The loudness level of any sound in "phons" is defined as being equal to the sound-pressure level of an equally loud, 1-kiloHertz tone. Thus, the loudness L and loudness level L of any sound are interrelated with the sound-pressure level S_1 of an equally loud, 1-kiloHertz tone according to

$$L = \text{antilog}_{10} [\alpha (L - 40)/10]$$
$$L = S_1$$

where α is a constant (experimentally $1/3 \leqslant \alpha \leqslant 1/2$).

The proposed method appears to be the only one which has, with good absolute accuracy, predicted the loudness and relative loudness of noises as judged by listeners.

This method should have application for prediction of loudness for a wide variety of situations such as noise suppression of jet engines, automobiles, trucks, and machinery, and for use in broadcasting, sound reproduction, speech analysis, and hearing aids.

The following documentation may be obtained from:

National Technical Information Service
Springfield, Virginia 22151
Single document price $3.00
(or microfiche $1.45)

Reference: NASA TM-X-2300, (N71-26993), Loudness Determined by Power Summation

Note:

The computer program for use with this method may be obtained from:

COSMIC
112 Barrow Hall
University of Georgia
Athens, Georgia 30601
Reference: LEW-11761

Source: Walton L. Howes
and Eileen A. LaSalvia
Lewis Research Center
(LEW-11761)

EFFECTS OF DECONTAMINATION, STERILIZATION, AND THERMAL VACUUM ON POLYMERIC PRODUCTS

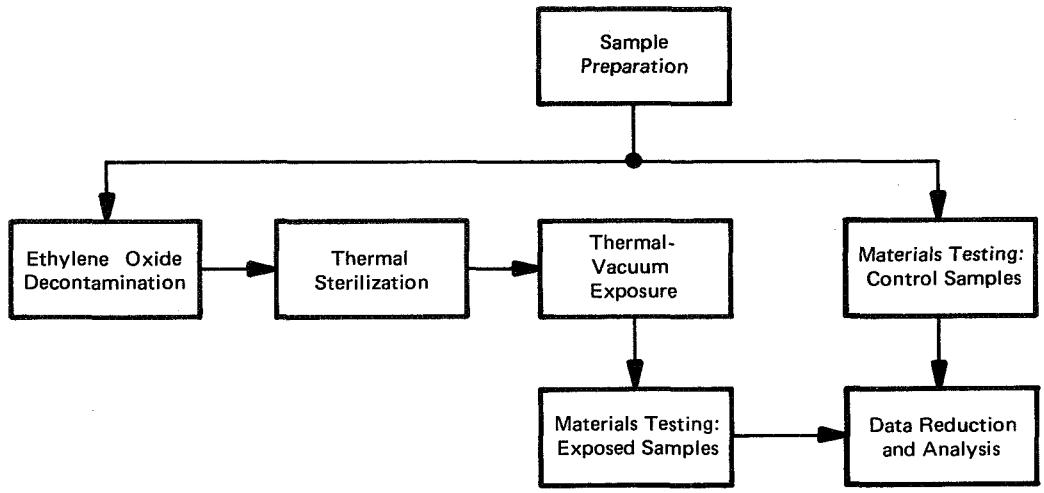

Exposure-and-Test Sequence

The effects of various sterilization environments on certain polymeric products have been determined. The eight material categories selected for this program were: (1) adhesives, (2) coatings, (3) coated fabrics, (4) elastomers, (5) encapsulants, (6) films, (7) hardware and structural materials, and (8) tapes. Each product was subjected to the following exposure sequence:

a. Six 30-hour decontamination cycles in a humidified ethylene oxide-freon atmosphere at 50° C,
b. Six 96-hour thermal-sterilization cycles in a dry nitrogen atmosphere at 135° C, and
c. One 500-hour thermal-vacuum exposure at 135° C and 10^{-6} torr.

The test sequence is outlined in the figure. Material properties were measured without exposure to the three environments (control specimens), as well as after exposure. The eleven physical, mechanical, and electrical tests employed for each class of material were as follows:

1. Adhesive shear strength,
2. Adhesion,
3. Adhesive creep,
4. Weight change,
5. Volume resistivity,
6. Dielectric strength,
7. Breaking strength,
8. Dimensional change,
9. Tensile strength,
10. Tear strength, and
11. Hardness and compression set.

The test results indicated that, of the products tested, the epoxy and fluorocarbon materials were the least affected, and polyesters and polyurethanes were the most affected. Of the material categories, tapes and elastomeric products were affected the most by the exposures.

This study was conducted primarily on polymeric products for use on spacecraft, but it should also be of interest to designers of equipment with vacuum or heat applications relating to polymeric products.

The following documentation may be obtained from:
National Technical Information Service
Springfield, Virginia 22151
Single document price $3.00
(or microfiche $1.45)
Reference: NASA-CR-103426 (N69-31924), Effects of Decontamination, Sterilization, and Thermal Vacuum on Spacecraft Polymeric Products.

Source: W. D. Roper of
Caltech/JPL
under contract to
NASA Pasadena Office
(NPO-11250)

DISCHARGE COEFFICIENTS FOR THICK-PLATE ORIFICES

Experimental discharge coefficients have been obtained for thick-plate orifices with approaching airflow perpendicular or inclined to the orifice axis. Other variables investigated were flow temperature and pressure; orifice pressure differential; approach Mach number; orifice diameter, thickness, and inlet edge radius; orifice surface finish; interference of multiple orifices; and approach passage geometry and length.

This investigation was undertaken to enable more accurate prediction of coolant flows within internally cooled turbine blades and vanes. The data should have broad applicability for predicting flows in designs where flow passages become comparatively complex.

The discharge coefficients (ratio of actual flow to ideal flow) were correlated with a velocity-head parameter which consisted of the ratio of the velocity head of the flow through the orifice to the velocity head of the flow approaching the orifice axis for various approach Mach numbers. The discharge coefficients were found to be dependent on the angle between the approaching flow and the axis of the orifice; on the ratio of the orifice thickness to orifice diameter; and on the inlet edge radius of the orifice. Also, the discharge coefficients were found to depend strongly on the approach Mach number and the static pressure difference across the orifice. The effects of flow temperature and pressure levels, orifice surface finish, multiple orifice interference, and approach passage geometry and length on discharge coefficients were found to be negligible for the cases considered.

The geometry of the main flow duct, in all cases but one, was a 0.25-in. (0.635-cm) diameter tube. (The exception was a rectangular cross-section main duct used to investigate the effect of curvature of the upstream face of the orifice.) The orifice thickness varied from 0.06 to 0.25 in. (0.15 to 0.635 cm) and the orifice diameters varied from 0.059 to 0.128 in. (0.150 to 0.325 cm). The inlet edge of the orifice was varied from a sharp corner to 0.030 in. (0.076 cm) radius. The main duct inlet airflow Mach number was varied from 0 to 0.65, static pressure was varied from 20.0 to 80.0 psia (138×10^3 to 552×10^3 N/m^2) and the temperature was varied from ambient to approximately 1000° F (810 K). Orifices with axes at 45° and 90° angles to the main duct flow were investigated.

The following documentation may be obtained from:

National Technical Information Service
Springfield, Virginia 22151
Single document price $6.00
(or microfiche $1.45)

Reference: NASA-TN-D-5467 (N69-38012), Discharge Coefficients for Thick Plate Orifices with Approach Flow Perpendicular and Inclined to the Orifice Axis.

Source: J. E. Rohde, H. T. Richards, and
G. W. Metger
Lewis Research Center
(LEW-11067)

Patent Information

The following innovations, described in this Compilation, have been patented or are being considered for patent action as indicated below:

Operation of a Nude Quadrupole Residual Gas Analyzer at Extended Cable Lengths (Page 2) MFS-22147

Inquiries concerning rights for the commercial use of this invention should be addressed to:

Patent Counsel
Marshall Space Flight Center
Code A&PS-PAT
Marshall Space Flight Center, Alabama 35812

Gas-Chromatographic Method for Analysis of Dissolved Oxygen (Page 5) MFS-22352

Inquiries concerning rights for the commercial use of this invention should be addressed to:

Patent Counsel
Marshall Space Flight Center
Code A&PS-PAT
Marshall Space Flight Center, Alabama 35812

Two-Stage Gas/Plasma Projectile Acceleration (Page 6) MFS-22145, 22287

This invention is owned by NASA, and a patent application has been filed. Inquiries concerning nonexclusive or exclusive license for its commercial development should be addressed to:

Patent Counsel
Marshall Space Flight Center
Code A&PS-PAT
Marshall Space Flight Center, Alabama 35812

Dichromatic Attenuation Method for Determining Bone-Mineral Mass *In Vivo* (Page 7) MSC-14276

Inquiries concerning rights for the commercial use of this invention should be addressed to:

Patent Counsel
Johnson Space Center
Code AM
Houston, Texas 77058